

Two-Port Feedback Analysis On Miller-Compensated Amplifiers

Myungjun Kim, *Member, IEEE*

Abstract—In this paper, various Miller-compensated amplifiers are analyzed by using the two-port feedback analysis together with the root-locus diagram. The proposed analysis solves problems of Miller theorem/approximation that fail to predict a pole-splitting and that require an impractical assumption that an initial lower frequency pole before connecting a Miller capacitor in a two-stage amplifier should be associated with the input of the amplifier. Since the proposed analysis sheds light on how the closed-loop poles originate from the open-loop poles in the s -plane, it allows the association of the closed-loop poles with the circuit components and thus provides a design insight for frequency compensation. The circuits analyzed are two-stage Miller-compensated amplifiers with and without a current buffer and a three-stage nested Miller-compensated amplifier.

Index Terms—Operational amplifier, Miller theorem, stability, frequency compensation, poles and zeros, two-port feedback analysis, root-locus diagram.

I. INTRODUCTION

MILLER theorem converts a feedback circuit into an open-loop circuit, allowing the association of the poles with the circuit nodes, which thus provides a design insight for frequency compensation. However, Miller theorem requires an impractical condition that the voltage-gain transfer function $a(s) = V_2/V_1$ in a given two-port network to be independent of $Y(s)$ which is an admittance connected across the ports [1]. For example, consider a two-stage amplifier in Fig. 1(a) where R_1 and C_1 (R_2 and C_2) model the impedance at the input (output) and C_c is a compensation capacitor. Since $Y(s) = sC_c$ and $a(s) = -K < 0$ which is independent of $Y(s)$, the Miller theorem can be applied to this circuit. However, because a transistor is used to achieve the voltage-gain from the input to output in practice, the circuit should be modeled by using a controlled current source with a transconductance g_m as shown in Fig. 1(b). Then, $a(s) = -g_m R_2 (1 - sC_c/g_m) / [1 + s(C_2 + C_c)R_2]$ is a function of $Y(s)$; thus, Miller theorem cannot be applied to this circuit.

Alternatively, Miller approximation using a dc value of $a(s)$, $|a(0)| = g_m R_2$, is often used to achieve the open-loop circuit as shown in Fig. 1(c). Assuming an initial lower frequency pole before connecting C_c is associated with the input of the amplifier (i.e., $|p_{o1}| = 1/R_1 C_1 < |p_{o2}| = 1/R_2 C_2$), the Miller approximation predicts that the input pole moves to a lower frequency and is located such that $p_{c1} \approx -1/g_m R_1 R_2 C_c$ which is true. However, it also predicts that a pole associated with the output becomes p_{c2} with a lower frequency as well, which is in variance with a pole-splitting [See Fig. 1(d)].

Myungjun Kim is with Samsung Electronics, Hwaseong, Korea e-mail: phaedruss.kim@samsung.com.

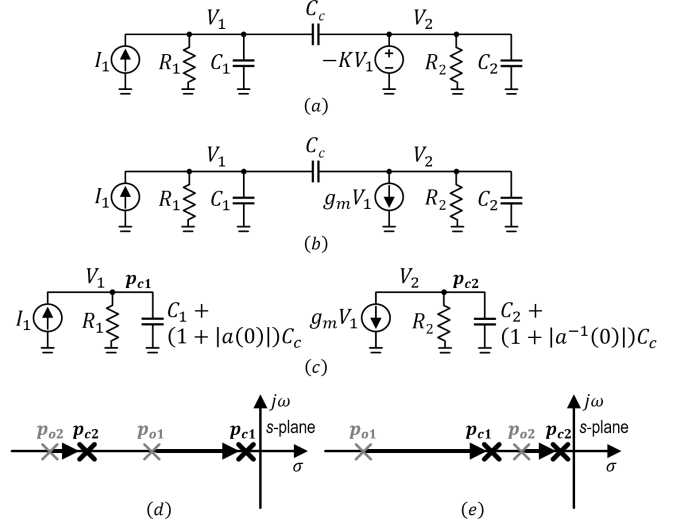


Fig. 1. Small-signal model of two-stage Miller-compensated amplifier using (a) controlled voltage source or (b) controlled current source. (c) Circuit obtained from applying Miller approximation to circuit in Fig. 1(b). Wrong estimation of the poles of circuit in Fig. 1(c) when the initial lower frequency pole before connecting C_c is at (d) V_1 node or (e) V_2 node.

Moreover, if the initial low-frequency pole is at the output (i.e., $|p_{o1}| = 1/R_1 C_1 > |p_{o2}| = 1/R_2 C_2$), which is a more general case because amplifiers are often required to drive a large load-capacitance, the Miller approximation predicts that the input pole moves to a lower frequency, which is completely false [See Fig. 1(e)]; the pole-splitting still occurs, implying the input pole moves to a higher frequency [1], which is very counter-intuitive.

On the other hand, the direct analysis (i.e., solving node equations to achieve the desired transfer function) provides accurate the pole/zero locations [2], [3]. However, it is so complex that the design insight for frequency compensation cannot be readily obtained.

In this paper, we use a two-port feedback analysis [4], [5] together with the root-locus diagram [6] to analyze two- and three-stage Miller-compensated amplifiers. This method solves the problems of Miller theorem/approximation mentioned above. Also, because the proposed analysis sheds light on how the closed-loop poles of the amplifier originated from the open-loop poles which can be readily found by inspection in the s -plane, it provides the design insight for frequency compensation.

This paper is organized as follows. Section II analyzes a simple two-stage Miller-compensated amplifier using the proposed method. Specifically, we will see that a non-dominant

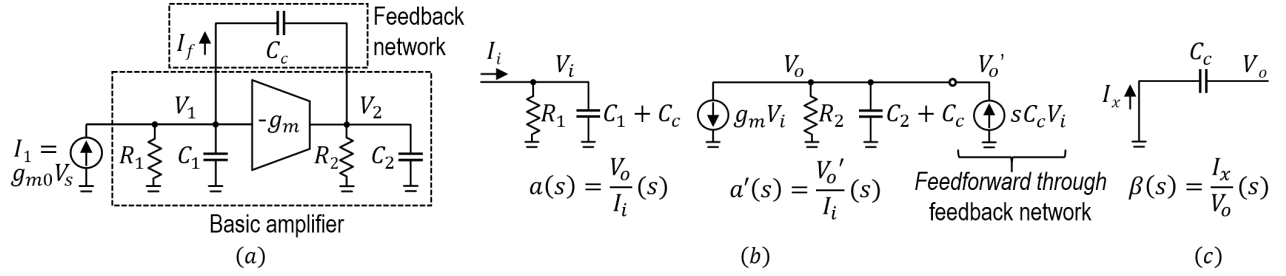


Fig. 2. (a) Two-stage Miller-compensated amplifier analyzed using two-port feedback analysis. (b) a -circuit. (c) β -circuit.

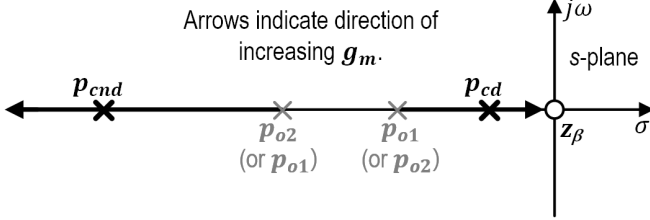


Fig. 3. Positive root-locus diagram for $a(s)\beta(s)$ given by (5). p_{o1} , p_{o2} are the poles of $a(s)\beta(s)$ or equivalently the poles of $A(s)$ when the feedback loop is *opened*. p_{cd} , p_{cnd} are respectively the possible dominant and non-dominant poles of $A(s)$ when the feedback loop is *closed*.

pole location in a classical textbook [4] should be modified to have a smaller magnitude when the right-half-plane (RHP) zero is neglected in the amplifier transfer function. Section III analyzes a two-stage Miller-compensated amplifier using a current buffer and shows that the stability can be improved due to the additional third-pole from the current buffer compared to the case without the current buffer. Section IV analyzes a three-stage nested Miller-compensated (NMC) amplifier [7]. Section V concludes the paper. Finally, appendices are included to present a pole-splitting theorem and perform the direct analysis to investigate the exact locations of the non-dominant poles in the NMC amplifier.

II. TWO-STAGE MILLER-COMPENSATED AMPLIFIER

A two-stage Miller-compensated amplifier is shown in Fig. 2(a). This circuit is a feedback transimpedance amplifier that has a shunt-shunt feedback topology where the basic amplifier and the feedback network are shown in the dashed boxes. Thus, it can be decomposed into a - and β -circuit as shown Fig. 2(b) and (c), respectively. Note that the a -circuit includes the loading effect of the feedback network. Also, note that there are two open-loop transimpedances with $[a'(s)]$ or without $[a(s)]$ a non-inverting current source $sC_c V_i$ at the output that models the feedforward current through C_c .

Let us first investigate $a(s)$. By inspection of Fig. 2(b),

$$\begin{aligned} a(s) &= \frac{V_o}{I_i}(s) \\ &= -\left(R_1 \parallel \frac{1}{s(C_1 + C_c)}\right) g_m \left(R_2 \parallel \frac{1}{s(C_2 + C_c)}\right) \\ &= -\frac{g_m R_1 R_2}{[1 + sR_1(C_1 + C_c)][1 + sR_2(C_2 + C_c)]} \end{aligned} \quad (1)$$

where $X \parallel Y = XY/(X + Y)$. Thus, $a(s)$ has two left-half-plane (LHP) real poles given by

$$p_{o1} = -\frac{1}{R_1(C_1 + C_c)} \quad (2)$$

$$p_{o2} = -\frac{1}{R_2(C_2 + C_c)} \quad (3)$$

where p_{o1} and p_{o2} are the open-loop poles associated with the input and output of the amplifier, respectively.

Next, $\beta(s)$ from Fig. 2(c) is given by

$$\beta(s) = \frac{I_x}{V_o}(s) = -sC_c. \quad (4)$$

Thus, $\beta(s)$ has a zero z_β at the origin (i.e., $z_\beta = 0$).

Combining (1) and (4), the $a(s)\beta(s)$ is given by

$$a(s)\beta(s) = \frac{g_m R_1 R_2 C_c s}{[1 + sR_1(C_1 + C_c)][1 + sR_2(C_2 + C_c)]}. \quad (5)$$

Using (5), we can draw the positive root-locus diagram for increasing g_m as shown in Fig. 3 to find the poles of the closed-loop transimpedance $A(s) = V_2/I_1$ in Fig. 2(a). Note that p_{o1} , p_{o2} are the poles of $a(s)\beta(s)$ or equivalently the poles of $A(s)$ when the feedback loop via C_c is *opened*, and p_{cd} , p_{cnd} are the possible dominant and non-dominant poles of $A(s)$ when the feedback loop via C_c is *closed*. And z_β is not a zero of $A(s)$ because it is from $\beta(s)$. Also note that the root-locus diagram includes the two cases where the initial lower frequency pole is either p_{o1} or p_{o2} . As can be readily seen, the root-locus diagram reveals the fact that p_{o1} and p_{o2} always split apart for increasing g_m irrespective of the condition about the initial low-frequency pole locations, which the Miller approximation fails to predict.

Let us now find the exact locations of the closed-loop pole p_{cd} , p_{cnd} . Since $a(s)\beta(s)$ has two LHP real and distinct poles, one zero at the origin and a large midband value¹ $a_0\beta_0$ assuming $g_m R_1$, $g_m R_2$ and C_c are large, we can apply the pole-splitting theorem presented in Appendix A. Depending on whether the initial lower frequency pole of $a(s)\beta(s)$ is p_{o1} or p_{o2} , $a_0\beta_0$ is expressed differently as

$$a_0\beta_0 = \begin{cases} \frac{g_m R_2 C_c}{C_1 + C_c} & \text{if } |p_{o1}| < |p_{o2}| \end{cases} \quad (6a)$$

$$a_0\beta_0 = \begin{cases} \frac{g_m R_1 C_c}{C_2 + C_c} & \text{if } |p_{o1}| > |p_{o2}|. \end{cases} \quad (6b)$$

¹The closed-loop poles are found from the midband value of $|a(j\omega)\beta(j\omega)|$ if $a(s)\beta(s)$ has zero(s) at the origin [8].

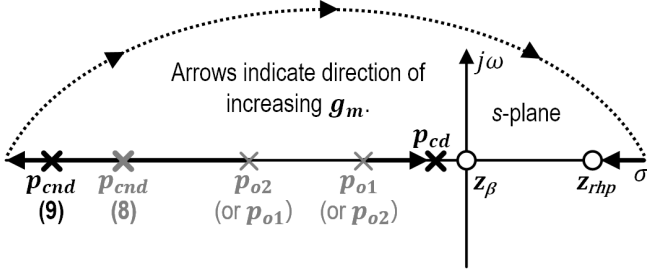


Fig. 4. Negative root-locus diagram for $a'(s)\beta(s)$.

Applying the pole-splitting relation (39) yields

$$p_{cd} \simeq -\frac{1}{g_m R_1 R_2 C_c} \quad (7)$$

$$p_{cnd} \simeq -\frac{g_m C_c}{(C_1 + C_c)(C_2 + C_c)}. \quad (8)$$

It should be mentioned that while the dominant pole p_{cd} given by (7) is the same as in [4], the non-dominant pole p_{cnd} given by (8) is in variance because

$$p_{cnd} \text{ in [4]} \simeq -\frac{g_m C_c}{(C_1 + C_c)(C_2 + C_c) - C_c^2}, \quad (9)$$

implying (8) is located at a lower frequency than (9). This variance is due to the assumption that the feedforward current through C_c is neglected. This is verified as follow. The exact transimpedance $A_{exact}(s) = V_2/I_1$ of the two-stage Miller-compensated amplifier in Fig. 2(a) is given by (10a). With some algebra, (10a) can be written in the form of the feedback equation as (10b). Comparing (10b) with (11a) obtained from the two-port feedback analysis shows that the only difference is that $(g_m - sC_c)$ has been replaced by g_m . Thus, such a deviation vanishes if we include the effect of $sC_c V_i$ current source in Fig. 2(b), yielding

$$\begin{aligned} a'(s) &= \frac{V'_o}{I_i}(s) \\ &= -\left(R_1 \parallel \frac{1}{s(C_1 + C_c)}\right) (g_m - sC_c) \left(R_2 \parallel \frac{1}{s(C_2 + C_c)}\right). \end{aligned} \quad (12)$$

Therefore, $A_{exact}(s) = a'(s)/[1 + a'(s)\beta(s)]$ as shown in (10b), validating the two-port feedback analysis.

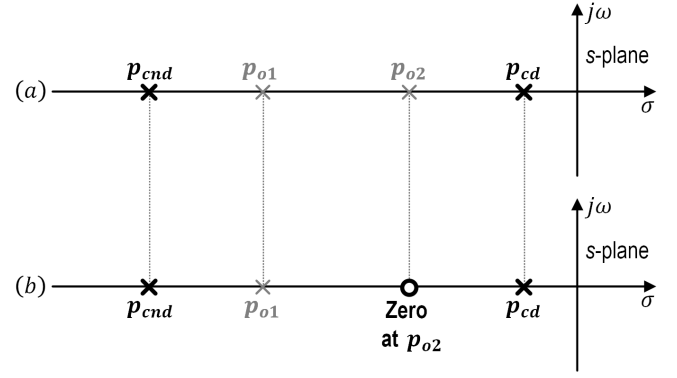


Fig. 5. Pole-zero diagram of (a) transimpedance V_2/I_1 and (b) input-impedance V_1/I_1 when $|p_{o1}| > |p_{o2}|$.

Indeed, *the non-dominant pole given by (8) is more accurate than (9) if the RHP zero ($z_{rhp} = g_m/C_c$) of the two-stage Miller-compensated amplifier is assumed to be at high frequency so as to be neglected.* z_{rhp} can be ignored by assuming a large g_m so that $(g_m - sC_c) \simeq g_m$ at the frequencies of interest. However, because the term $(g_m - sC_c)$ also exists in the denominator of (10b), such condition also alter the non-dominant pole location by modifying the coefficient of $s^2 R_1 R_2$ to include an additional term of C_c^2 as shown in the denominator of (11b), which results in (8) to have a smaller magnitude than (9).

Such increase in the magnitude of the non-dominant pole can also be explained using the root-locus diagram for $a'(s)\beta(s)$ as shown in Fig. 4. Note that the negative locus rule [6] is applied here because of the low-frequency sign reversal associated with the RHP zero [8]. Similar to Fig. 3, p_{cnd} moves toward high frequency in the LHP as g_m increases. However, it eventually moves into the RHP, manifesting itself at $s = z_{rhp}^+$ if $g_m \rightarrow \infty$; thus, for a given finite g_m , p_{cnd} is located at nearer to $s = -\infty$ when the RHP zero is included as illustrated in Fig. 4.

So far, we have investigated the pole/zero locations of the transimpedance V_2/I_1 of the circuit in Fig. 2(a). It is worth mentioning of the pole/zero locations of the input-impedance V_1/I_1 . Since the natural structure of the circuit is unchanged, p_{cd} , p_{cnd} are also unchanged. However, the voltage-amplifier

$$A_{exact}(s) = \frac{-(g_m - sC_c)R_1 R_2}{1 + s[R_1 C_1 + R_2 C_2 + (g_m R_1 R_2 + R_1 + R_2)C_c] + s^2 R_1 R_2 [C_1 C_2 + C_c(C_1 + C_2)]} \quad (10a)$$

$$= \frac{-\left(R_1 \parallel \frac{1}{s(C_1 + C_c)}\right) (g_m - sC_c) \left(R_2 \parallel \frac{1}{s(C_2 + C_c)}\right)}{1 + \left(R_1 \parallel \frac{1}{s(C_1 + C_c)}\right) (g_m - sC_c) \left(R_2 \parallel \frac{1}{s(C_2 + C_c)}\right) sC_c} = \frac{a'(s)}{1 + a'(s)\beta(s)} \quad (10b)$$

$$A(s) = \frac{-\left(R_1 \parallel \frac{1}{s(C_1 + C_c)}\right) g_m \left(R_2 \parallel \frac{1}{s(C_2 + C_c)}\right)}{1 + \left(R_1 \parallel \frac{1}{s(C_1 + C_c)}\right) g_m \left(R_2 \parallel \frac{1}{s(C_2 + C_c)}\right) sC_c} = \frac{a(s)}{1 + a(s)\beta(s)} \quad (11a)$$

$$= \frac{-g_m R_1 R_2}{1 + s[R_1 C_1 + R_2 C_2 + (g_m R_1 R_2 + R_1 + R_2)C_c] + s^2 R_1 R_2 [C_1 C_2 + C_c(C_1 + C_2) + C_c^2]} \quad (11b)$$

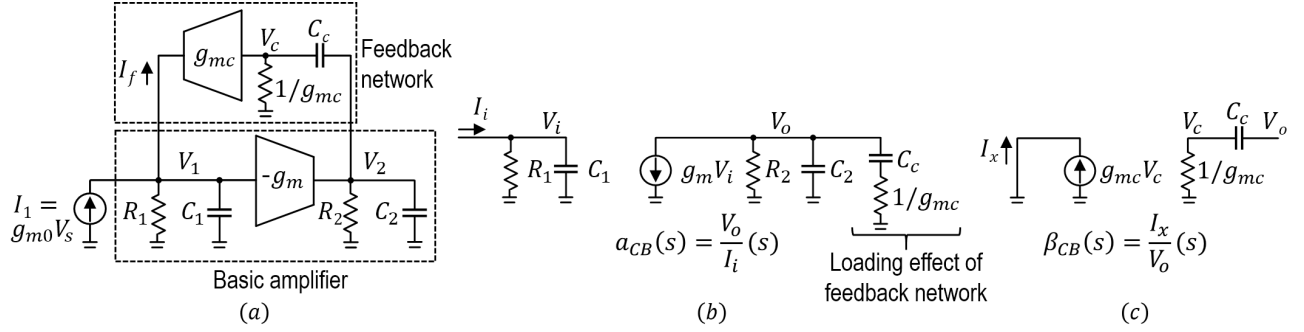


Fig. 6. (a) Two-stage Miller-compensated amplifier using current buffer analyzed using two-port feedback analysis. (b) a -circuit. (c) β -circuit.

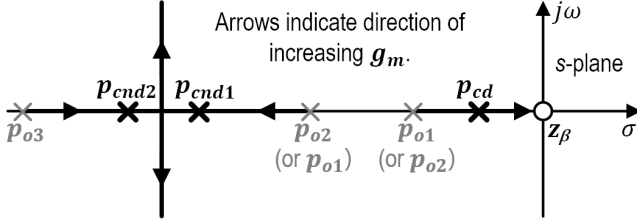


Fig. 7. Positive root-locus diagram for $a_{CB}(s)\beta_{CB}(s)$ given by (20). p_{o1} , p_{o2} and p_{o3} are the poles of $a_{CB}(s)\beta_{CB}(s)$ or equivalently the poles of $A_{CB}(s)$ when the feedback loop is opened. Also, p_{cd} , p_{cnd1} and p_{cnd2} are respectively the possible dominant, first and second non-dominant poles of $A_{CB}(s)$ when the feedback loop is closed.

V_o/V_i or V'_o/V_i in Fig. 2(b) that has a pole p_{o2} is now included *not* in the basic amplifier *but* in the feedback network, and thus p_{o2} becomes a zero in the input-impedance. For example, the pole-zero diagram of the transimpedance V_2/I_1 , input-impedance V_1/I_1 when $|p_{o1}| > |p_{o2}|$ are shown in Fig. 5(a), (b), respectively. The pole/zero pattern of the input-impedance can be employed as a lag compensating network to control a damping factor of the complex poles in a three-stage amplifier in [9].

III. TWO-STAGE MILLER-COMPENSATED AMPLIFIER USING CURRENT BUFFER

The RHP zero in the Miller-compensated two-stage amplifier in the previous section was ignored by assuming a large g_m , which requires a large power consumption in practice. Instead, the RHP zero can be removed by employing a unilateral current buffer [10], [11] in the feedback network, allowing only a current through C_c to flow backward from the output to the input of the transistor (g_m) as shown in Fig. 6(a). Note that the feedback network now has a current buffer with an input impedance of $1/g_{mc}$ and the transconductance g_{mc} . Since this circuit also has a shunt-shunt feedback topology, it can be decomposed into a - and β -circuit as shown Fig. 6(b) and (c), respectively. Note that unlike the amplifier without the current buffer, the feedback loading only occurs at the output of the amplifier in the a -circuit.

Assuming $g_{mc}R_2 \gg 1$, the open-loop transimpedance

$a_{CB}(s)$ is

$$a_{CB}(s) = \frac{V_o}{I_i}(s) = -\frac{g_m R_1 R_2 (1 + sC_c/g_{mc})}{[1 + sR_1 C_1][1 + sR_2(C_2 + C_c)][1 + s\frac{C_2 \parallel C_c}{g_{mc}}]} \quad (13)$$

Thus, $a_{CB}(s)$ has three LHP real poles as

$$p_{o1} = -\frac{1}{R_1 C_1} \quad (14)$$

$$p_{o2} = -\frac{1}{R_2(C_2 + C_c)} \quad (15)$$

$$p_{o3} = -\frac{g_{mc}}{C_2 \parallel C_c} \quad (16)$$

and one LHP zero as

$$z_a = -\frac{g_{mc}}{C_c} \quad (17)$$

From Fig. 6(c), $\beta_{CB}(s)$ is

$$\beta_{CB}(s) = \frac{I_x}{V_o}(s) = -\frac{sC_c}{1 + sC_c/g_{mc}} \quad (18)$$

Thus, $\beta_{CB}(s)$ has one LHP real pole as

$$p_\beta = -\frac{g_{mc}}{C_c} \quad (19)$$

and a zero $z_\beta = 0$.

Since (19) coincides with (17), the $a_{CB}(s)\beta_{CB}(s)$ has the three LHP poles, a zero z_β at the origin, and is expressed as

$$a_{CB}(s)\beta_{CB}(s) = \frac{g_m R_1 R_2 C_c s}{[1 + sR_1 C_1][1 + sR_2(C_2 + C_c)][1 + s\frac{C_2 \parallel C_c}{g_{mc}}]} \quad (20)$$

The positive root-locus diagram of $a_{CB}(s)\beta_{CB}(s)$ for increasing g_m is shown in Fig. 7. The resulting loci indicate the locations of the poles of the closed-loop transimpedance $A_{CB}(s) = V_2/I_1$ in Fig. 6(a). As g_m increases, p_{o1} and p_{o2} split apart and become the dominant pole p_{cd} and the first non-dominant pole p_{cnd1} , respectively. Also, p_{o3} moves toward lower frequency and becomes the second non-dominant pole p_{cnd2} for increasing g_m , implying that p_{cnd1} and p_{cnd2} can form a complex pole pair beyond some value of g_m . Thus, we should analyze how effective this amplifier is compared to the

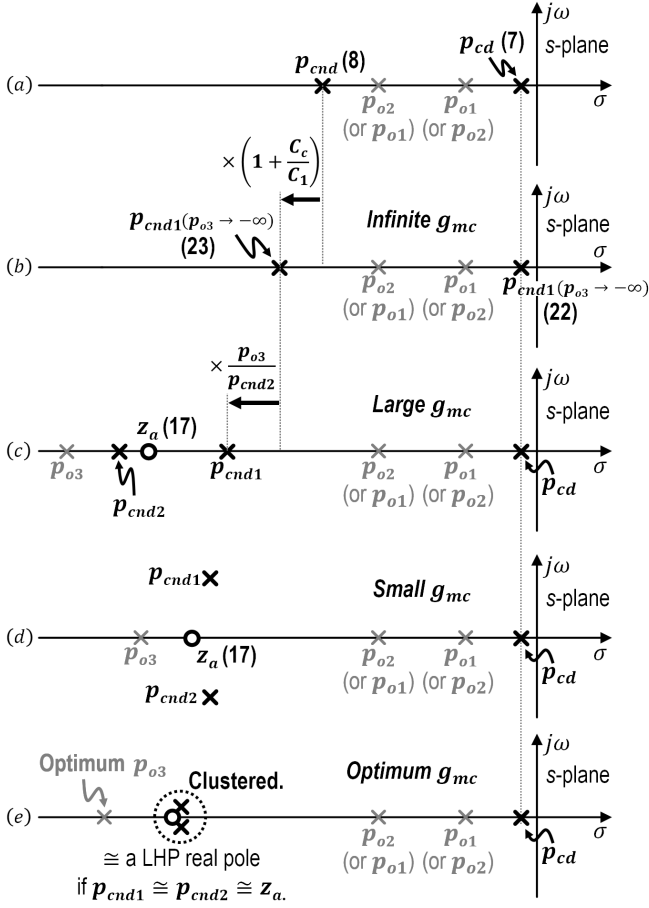


Fig. 8. Pole-zero diagram of the closed-loop transimpedance V_2/I_1 of the two-stage amplifier (Not to scale): (a) without current buffer, (b) with ideal current buffer that has infinite g_{mc} , (c) with non-ideal current buffer that has large g_{mc} , (d) with non-ideal current buffer that has small g_{mc} , (e) with non-ideal current buffer that has optimum g_{mc} .

previous amplifier in Section II and also investigate the effect of the third pole p_{o3} on the stability of the amplifier.

First, let us compare the Miller compensated amplifier using the current buffer with the previous amplifier by assuming that $p_{o3} \rightarrow -\infty$ so as to be neglected. It is achieved by assuming the ideal current buffer with zero input impedance (i.e., $g_{mc} \rightarrow \infty$). Then, (20) reduces to have the two LHP poles, a zero at the origin and the midband value $a_0\beta_0|_{CB}$ as

$$a_0\beta_0|_{CB} = \begin{cases} \frac{g_m R_2 C_c}{C_1} & \text{if } |p_{o1}| < |p_{o2}| \\ \frac{g_m R_1 C_c}{C_2 + C_c} & \text{if } |p_{o1}| > |p_{o2}|. \end{cases} \quad (21a)$$

$$(21b)$$

Since the midband value is typically very large, we apply the pole-splitting theorem in Appendix A to find the splitted

closed-loop poles as

$$p_{cd(p_{o3} \rightarrow -\infty)} \simeq -\frac{1}{g_m R_1 R_2 C_c} \quad (22)$$

$$p_{cnd1(p_{o3} \rightarrow -\infty)} \simeq -\frac{g_m}{C_2 + C_c} \frac{C_c}{C_1}. \quad (23)$$

While the dominant pole (22) is the same with (7), the non-dominant pole given by (23) is located at higher frequency than (8) by a multiplication factor of $1 + C_c/C_1$ which is typically large because C_1 is a small parasitic capacitance. Thus, the amplifier with the current buffer has the better relative stability than the amplifier without the current buffer if their gain-bandwidth products (GBWs) are the same.² The pole-zero diagrams of the transimpedance V_2/I_1 of the two-stage amplifier without the current buffer and the two-stage amplifier with the ideal current buffer is shown in Fig. 8(a), (b), respectively.

Such increase of magnitude of the non-dominant pole is explained as follows. When $|p_{o1}| < |p_{o2}|$, (21a) is larger than (6a) by the multiplication factor of $1 + C_c/C_1$; thus, such increased midband value help move p_{o2} given by (15) to become p_{cnd1} that is located at higher frequency than (8). When $|p_{o1}| > |p_{o2}|$, though the midband value given by (21b) is unchanged compared to (6b), the initial higher frequency pole p_{o1} given by (14) is located at more higher frequency than (2) by the multiplication factor of $1 + C_c/C_1$ because the loading effect does not occur at the input of the amplifier; thus, p_{cnd1} is located at higher frequency than (8) as well.

Next, we consider a non-ideal current buffer that has a finite g_{mc} so that p_{o3} and thus p_{cnd2} are not neglected. Assuming $g_m, g_{mc} \gg 1/R_1, 1/R_2$; $C_c, C_2 \gg C_1$; $g_m R_1 \gg C_2/C_c$, $A_{CB}(s)$ is given by (24) at the bottom of the page. Note that the dominant pole p_{cd} is the same as (22); this is because p_{o1} is typically located at much lower frequency than p_{o3} and thus $|a_{CB}(j\omega)\beta_{CB}(j\omega)|$ at $\omega = |p_{o1}|$ is little affected by p_{o3} . Therefore, p_{o1} moves toward the origin for the same amount and becomes p_{cd} as before when feedback-loop is closed for a given g_m .

The other poles p_{cnd1} , p_{cnd2} can be found by factoring the second-order polynomial in the denominator of $A_{CB}(s)$. Though simple expressions for p_{cnd1} , p_{cnd2} cannot be readily generated, they have the following simple relation:

$$p_{cnd1} p_{cnd2} = \frac{g_m g_{mc}}{C_1 C_2}. \quad (25)$$

²GBWs of the voltage-gain V_2/V_s of the amplifier in Fig. 2(a) and Fig. 6(a) are expressed as g_{m0}/C_c by replacing the input current source I_1 with $g_{m0}V_s$ where g_{m0} is an additional input transconductance applied to the input voltage V_s .

$$A_{CB}(s) = \frac{a_{CB}(s)}{1 + a_{CB}(s)\beta_{CB}(s)} \simeq \frac{-g_m R_1 R_2 \left(1 + s \frac{C_c}{g_{mc}}\right)}{(1 + s g_m R_1 R_2 C_c) \left(1 + s \frac{C_c C_2 + g_{mc} R_1 C_1 (C_c + C_2)}{g_m R_1 g_{mc} C_c} + s^2 \frac{C_1 C_2}{g_m g_{mc}}\right)} \quad (24)$$

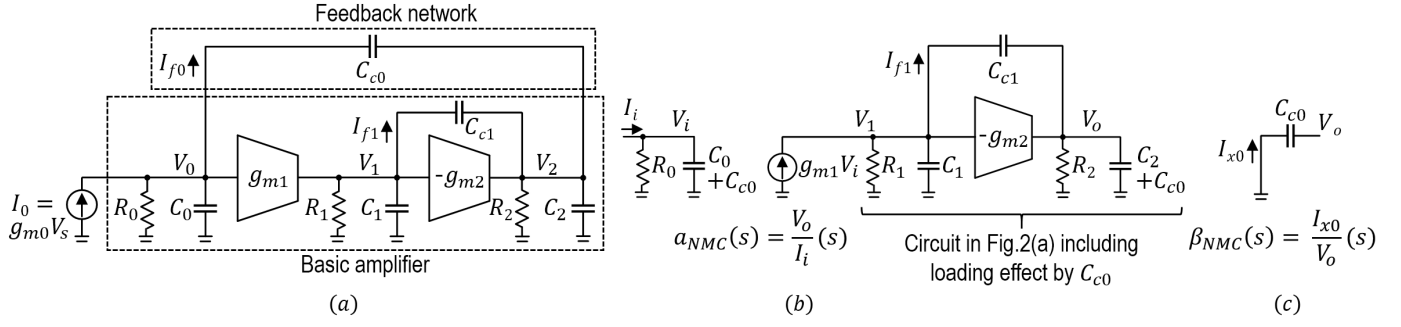


Fig. 9. (a) Three-stage NMC amplifier analyzed using two-port feedback analysis. (b) a -circuit. (c) β -circuit.

Since the right-hand side of (25) can be obtained by multiplying (16) with (23), we write

$$p_{cnd1} = \frac{p_{o3}}{p_{cnd2}} p_{cnd1(p_{o3} \rightarrow -\infty)}. \quad (26)$$

Thus, p_{cnd1} is modified with a multiplication factor of p_{o3}/p_{cnd2} compared to $p_{cnd1(p_{o3} \rightarrow -\infty)}$. Let us consider the following two cases where g_{mc} and thus p_{o3} (16) are different but the midband values of $a_{CB}(s)\beta_{CB}(s)$ are preserved since (21a) and (21b) are not functions of g_{mc} : 1) g_{mc} is large and thus p_{o3} is located at high frequency so that p_{cnd1} and p_{cnd2} are real and 2) g_{mc} is small and thus p_{o3} is located at low frequency so that p_{cnd1} and p_{cnd2} are complex.

1) When g_{mc} is large so that p_{cnd1} and p_{cnd2} are real, p_{o3}/p_{cnd2} is obviously larger than "1" as shown in the root-locus diagram in Fig. 7; thus, p_{cnd1} is located at higher frequency than $p_{cnd1(p_{o3} \rightarrow -\infty)}$ as if attracted by p_{cnd2} as shown in the pole-zero diagram of V_2/I_1 in Fig. 8(c). Note that because z_a (17) is the zero of $a_{CB}(s)$ and p_β (19) is not the pole of $a_{CB}(s)\beta_{CB}(s)$, a zero z_a exists in $A_{CB}(s)$. Though p_{cnd2} is at the lower frequency than in the previous ideal current buffer case, the stability is not degraded if z_a and p_{cnd2} are closely spaced so as to be canceled as shown in Fig. 8(c). Thus, this case is better than the Miller compensation with the ideal current buffer since it achieves both the improved stability margin and the lower power consumption with the finite g_{mc} .

2) When g_{mc} is small so that p_{cnd1} and p_{cnd2} are complex, the magnitude of the complex poles is still larger than that of $p_{cnd1(p_{o3} \rightarrow -\infty)}$ [13]. Thus, power consumption can be further reduced by decreasing g_{mc} compared to the previous real non-dominant poles case without deteriorating the stability. However, since a real part of the complex pole-pair is fixed at $s \simeq p_{o3}/2$, too small g_{mc} can result in a small damping ratio of the pole-pair, degrading stability margins shown in Fig. 8(d). Therefore, for a given g_m , an optimum design that achieves both good stability and low power consumption can be achieved by locating p_{o3} with the optimum g_{mc} , allowing

p_{cnd1} and p_{cnd2} to be located at near z_a so that they can be considered a LHP real pole as shown in Fig. 8(e) (i.e., $p_{c2} \simeq p_{cM} \simeq z_a$).

IV. THREE-STAGE NMC AMPLIFIER

In this section, we analyze three-stage NMC amplifiers [7] by using two-port feedback analysis.

A three-stage NMC amplifier is shown in Fig. 9(a). Note that two Miller capacitors C_{c0} , C_{c1} are employed and the input current source I_0 is expressed as $g_{m0}V_s$ where V_s is the input voltage of the NMC amplifier. Also, note that a two-stage Miller-compensated amplifier in Section II is included in this NMC amplifier. This circuit is also a feedback transimpedance amplifier that has a shunt-shunt feedback topology where the basic amplifier and the feedback network are shown in the dashed boxes in Fig. 9(a). Thus, it can be decomposed into a - and β -circuit as shown Fig. 9(b) and (c), respectively. It should be noted that the a -circuit is drawn by neglecting the signal feedforward through C_{c0} for simplicity. Also, the a -circuit includes the two-stage amplifier in Fig. 2(a) where the output impedance includes the loading effect by C_{c0} .

Using the same approaches and the results in Section II, $a_{NMC}(s)\beta_{NMC}(s)$ which is given by (27) shown at the bottom of the page has three LHP poles given by

$$p_{o0} = -\frac{1}{R_0(C_0 + C_{c0})} \simeq -\frac{1}{R_0C_{c0}} \quad (28)$$

$$p_{o1} = -\frac{1}{g_{m2}R_1R_2C_{c1}} \quad (29)$$

$$p_{o2} = -\frac{g_{m2}C_{c1}}{(C_1 + C_{c1})(C_2 + C_{c0} + C_{c1})} \simeq -\frac{g_{m2}}{C_2} \quad (30)$$

where the approximations in (28) and (30) follow if $C_2 \gg C_{c0}, C_{c1} \gg C_0, C_1$ since typically C_2 is a large load capacitance and C_0, C_1 are small parasitics. Also, $a_{NMC}(s)\beta_{NMC}(s)$ has a z_β at the origin from the $\beta_{NMC}(s) = I_{f0}/V_o$ in Fig. 9(c). Note that p_{o1} and p_{o2} are expressed by neglecting the signal feedforward through C_{c1} .

$$a_{NMC}(s)\beta_{NMC}(s) = \frac{g_{m1}g_{m2}R_0R_1R_2C_{c0}s}{[1 + sR_0(C_0 + C_{c0})][1 + sg_{m2}R_1R_2C_{c1}] \left[1 + s \frac{(C_1 + C_{c1})(C_2 + C_{c0} + C_{c1})}{g_{m2}C_{c1}} \right]} \quad (27)$$

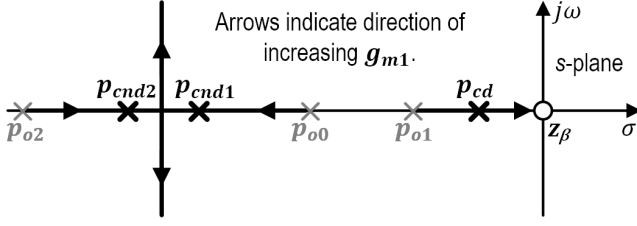


Fig. 10. Positive root-locus diagram for $a_{NMC}(s)\beta_{NMC}(s)$ given by (27). p_{o0} , p_{o1} and p_{o2} are the poles of $a_{NMC}(s)\beta_{NMC}(s)$ or equivalently the poles of $A_{NMC}(s) = V_2/I_0$ when the feedback loop via C_{c0} is opened. Also, p_{cd} , p_{cnd1} and p_{cnd2} are respectively the possible dominant, first and second non-dominant poles of $A_{NMC}(s)$ when the feedback loop via C_{c0} is closed.

Typically, $|p_{o1}| < |p_{o0}| < |p_{o2}|$ because of a large g_{m2} in the design of the NMC amplifier [2]. Thus, the positive root-locus diagram for increasing g_{m1} can be drawn as shown in Fig. 10. As can be seen, the two low frequency poles p_{o1} and p_{o0} split apart as g_{m1} increases and become a dominant pole p_{cd} and a first non-dominant pole p_{cnd1} , respectively. It should also be noted that p_{o2} moves toward low frequency and becomes a second non-dominant pole p_{cnd2} as g_{m1} increases. Also, note that p_{cnd1} and p_{cnd2} can form a complex-conjugate pole-pair beyond some value of g_{m1} .

Using a similar approach in the Section III, let us first assume p_{o2} is located at very high frequency so as to be neglected and investigate a dominant (p_{cd}) and a first non-dominant (p_{cnd1}) pole locations; in this case, (27) can be approximated to have the two LHP poles, a zero at the origin, and a midband value $a_0\beta_0|_{NMC}$ as given by

$$a_0\beta_0|_{NMC} = \frac{g_{m1}R_0C_{c0}}{C_{c1}} \quad (31)$$

which is typically large. Thus, the splitted closed-loop poles can be found by applying the pole-splitting relation (39), which results in

$$p_{cd(p_{o2} \text{ at HF})} \simeq -\frac{1}{g_{m1}g_{m2}R_0R_1R_2C_{c0}} \quad (32)$$

$$p_{cnd1(p_{o2} \text{ at HF})} \simeq -\frac{g_{m1}}{C_{c1}} \quad (33)$$

Thus, GBW of this NMC amplifier is g_{m0}/C_{c0} . Typically, a magnitude of the first non-dominant pole given by (33) is set to be

$$\frac{g_{m1}}{C_{c1}} = 2\text{GBW} = 2\frac{g_{m0}}{C_{c0}} \quad (34)$$

so that the phase margin (PM) $\simeq 90^\circ - \tan^{-1}(1/2) \simeq 63^\circ$ [2]; the pole-zero diagram of the voltage-gain of this NMC amplifier is illustrated in Fig. 11(a). It is worth mentioning that the proposed analysis shows that p_{o2} should be located at a high frequency such that $|p_{o2}| = |p_{cnd2}| \gg \text{GBW}$ to satisfy

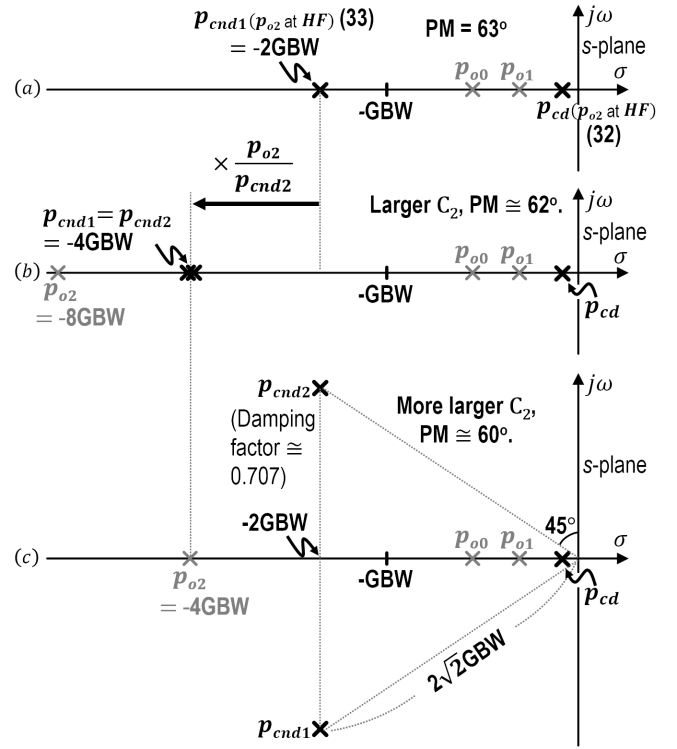


Fig. 11. Pole-zero diagram of the voltage-gain V_2/V_s of the three-stage NMC amplifier (Not to scale): (a) when p_{o2} is located at a very high frequency so as to be neglected, (b) when p_{o2} is located at $s = -8\text{GBW}$, and (c) when p_{o2} is located at $s = -4\text{GBW}$.

(34), implying a separate pole approach in [2] that satisfies not only (34) but $|p_{cnd2}| = 2\text{GBW}$ cannot be achieved.

Next, we consider the case when p_{o2} is located at a lower frequency and investigate its effect on the stability. Though this can be achieved by decreasing g_{m2} , it will also affect p_{o1} given by (29). Instead, increasing C_2 only allows p_{o2} to be located at a lower frequency. Then, as mentioned earlier, p_{o2} moves toward low frequency and becomes the second-nondominant pole p_{cnd2} . Similar to the case in the Miller compensated two-stage using the non-ideal current buffer in Section III, the first non-dominant pole p_{cnd1} here is at a higher frequency than (33) as if attracted by p_{cnd2} . This is verified as follows.

Assuming $g_{m1}, g_{m2} \gg 1/R_0, 1/R_1, 1/R_2$; $C_2 \gg C_{c0}, C_{c1} \gg C_0, C_1$; $A_{NMC}(s) = V_2/I_0$ in Fig. 9(a) is approximately expressed as (35) shown at the bottom of the page. From a quadratic function in the denominator of (35), p_{cnd1} and p_{cnd2} have the following relation:

$$p_{cnd1}p_{cnd2} \simeq \frac{g_{m1}g_{m2}}{C_{c1}C_2}. \quad (36)$$

Because the right-hand side of (36) can also be obtained by

$$A_{NMC}(s) = \frac{V_2}{I_0}(s) = \frac{a_{NMC}(s)}{1 + a_{NMC}(s)\beta_{NMC}(s)} \simeq \frac{-g_{m1}g_{m2}R_0R_1R_2}{(1 + sg_{m1}g_{m2}R_0R_1R_2C_{c0}) \left[1 + s\frac{C_{c1}}{g_{m1}} + s^2\frac{C_{c1}C_2}{g_{m1}g_{m2}} \right]} \quad (35)$$

multiplying (30) with (33), we can write

$$p_{cnd1} \simeq \frac{p_{o2}}{p_{cnd2}} p_{cnd1(p_{o2} \text{ at } HF)}. \quad (37)$$

Thus, p_{cnd1} is located at higher frequency than $p_{cnd1(p_{o2} \text{ at } HF)}$ by a multiplication factor of p_{o2}/p_{cnd2} that is obviously larger than unity as shown in the root-locus diagram in Fig. 10. This implies that *even if p_{o2} is not located at very high frequency, the stability margin may be little affected by p_{cnd2} because the magnitude of p_{cnd1} is also increased.*

For example, we consider two cases that have different values of C_2 so that 1) $p_{o2} = -8\text{GBW}$, and 2) $p_{o2} = -4\text{GBW}$ and the condition (34) holds in the both cases. The exact analysis is carried out for the both cases in Appendix B.

1) When $p_{o2} = -8\text{GBW}$, the NMC amplifier has the pole-zero diagram as illustrated in Fig. 11(b). Note that the dominant pole p_{cd} is at the same location as in the previous case because p_{o1} is typically located at much lower frequency than p_{o2} and thus $|a_{NMC}(j\omega)\beta_{NMC}(j\omega)|$ at $\omega = |p_{o2}|$ is little affected by p_{o2} . However, p_{o0} and p_{o2} attract each other, becoming the first (p_{cnd1}) and second non-dominant (p_{cnd2}) pole, and form a double pole-pair at $s = -4\text{GBW}$, which results in $PM \simeq 90^\circ - 2\tan^{-1}(1/4) \simeq 62^\circ$. Thus, the stability of the NMC amplifier is little affected compared to the previous case.

2) When $p_{o2} = -4\text{GBW}$, the NMC amplifier has the pole-zero diagram as illustrated in Fig. 11(c). The location of p_{cd} is still the same as the previous cases. However, p_{cnd1} and p_{cnd2} form a complex-conjugate pole-pair that has the same magnitude of the real- and imaginary-part as 2GBW (i.e., $|p_{cnd1}| = |p_{cnd2}| = 2\sqrt{2}\text{GBW}$) with a damping ratio (ξ) of $1/\sqrt{2} \simeq 0.707$, which results in

$$PM \simeq 90^\circ - \tan^{-1} \left[\frac{2\xi \frac{GBW}{2\sqrt{2}GBW}}{1 - \left(\frac{GBW}{2\sqrt{2}GBW}\right)^2} \right] \simeq 60^\circ. \quad (38)$$

Thus, the stability of the NMC amplifier is also little affected compared to the previous cases.

V. CONCLUSION

In this paper, various Miller-compensated amplifiers are analyzed by using the two-port feedback analysis together with the root-locus diagram. This method solves the problems of Miller theorem/approximation that fail to predict the pole-splitting and that requires an impractical assumption where an initial low-frequency pole before connecting a Miller capacitor in a multi-stage amplifier should be associated with the input of the amplifier. Also, because the proposed analysis sheds light on how the closed-loop poles of the amplifier originated from the open-loop poles which can be readily found by inspection in the s -plane, it provides the design insight for frequency compensation, helping allow the association of the closed-loop poles with the circuit parameters.

Specifically, in Section II, the proposed analysis shows that when the RHP zero is neglected the nondominant pole location of the two-stage Miller-compensated amplifier should be modified to have a smaller magnitude than in a classical textbook [4]. Also, in Section III, when the current buffer is

used in a Miller compensated two-stage amplifier to block the feedforward path through the compensation capacitor, the stability can be improved because of the absence of the RHP zero and the loading effect of compensation capacitor at the input of the amplifier. Moreover, the additional third pole from the current buffer and the zero of the a -circuit can be optimally located to improve the stability and to lower the power consumption. Finally, in Section IV, the stability of the three-stage NMC amplifier can be little affected even if the second non-dominant pole is considered because the first non-dominant pole is located at a higher frequency as if attracted by the second non-dominant pole.

APPENDIX A POLE-SPLITTING THEOREM

Let $a(s)\beta(s)$ of a feedback circuit has two distinct real poles, p_{od} and p_{ond} , in the left-half of the s -plane such that $|p_{od}| < |p_{ond}|$, a zero at the origin, and a midband value $a_0\beta_0 \gg 2$. Then, the following Pole-splitting relation holds:

$$\boxed{a_0\beta_0 \simeq \frac{p_{od}}{p_{cd}} \simeq \frac{p_{cnd}}{p_{ond}}} \quad (39)$$

where p_{cd} and p_{cnd} are the closed-loop poles of the circuit. ■

Proof: For a given condition, $a(s)\beta(s)$ can be written

$$a(s)\beta(s) = \frac{a_0\beta_0 \frac{s}{|p_{od}|}}{\left(1 + \frac{s}{|p_{od}|}\right) \left(1 + \frac{s}{|p_{ond}|}\right)}. \quad (40)$$

The closed-loop poles of the circuit [or equivalently the zeros of the characteristic equation $1 + a(s)\beta(s)$] can be found as the zeros of

$$P(s) = 1 + s \frac{a_0\beta_0}{|p_{od}|} + s^2 \frac{1}{|p_{od}p_{ond}|}. \quad (41)$$

The two zeros of $P(s)$, p_{cd} and p_{cnd} , are real and widely spaced (i.e., $|p_{cnd}| \gg |p_{cd}|$). This can be verified by comparing (41) with the standard form of the second-order polynomial with a damping ratio ξ and a natural frequency ω_n given by

$$S(s) = 1 + s \frac{2\xi}{\omega_n} + s^2 \frac{1}{\omega_n^2}. \quad (42)$$

Equating (41) with (42) yields

$$\xi = \frac{1}{2} \sqrt{\frac{p_{ond}}{p_{od}}} a_0\beta_0 > \frac{1}{2} a_0\beta_0 \gg 1. \quad (43)$$

Thus, we can write

$$P(s) \simeq 1 + s \frac{1}{|p_{cd}|} + s^2 \frac{1}{|p_{cd}p_{cnd}|}. \quad (44)$$

Equating the coefficient of s in (41) and (44) results in

$$|p_{cd}| \simeq \frac{|p_{od}|}{a_0\beta_0}. \quad (45)$$

Similarly, by equating coefficients of s^2 in (41) and (44) and using (45), p_{cnd} can be estimated as

$$|p_{cnd}| \simeq |p_{ond}| a_0\beta_0. \quad (46)$$

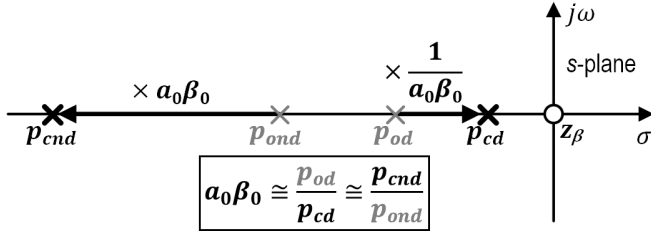


Fig. 12. Pole-splitting relation

Using (45), (46) and eliminating the absolute functions, the pole-splitting relation given by (39) is established and is illustrated in Fig. 12.

□

APPENDIX B

Applying the quadratic formula to the quadratic function in the denominator of (35), p_{cnd1} and p_{cnd2} are

$$p_{cnd1}, p_{cnd2} = -\frac{g_{m2}}{2C_2} \pm \frac{g_{m2}}{2C_2} \sqrt{1 - 4 \frac{g_{m1}}{C_{c1}} \frac{C_2}{g_{m2}}}. \quad (47)$$

Using (30) and (34), we can write

$$p_{cnd1}, p_{cnd2} \simeq \frac{p_{o2}}{2} \mp \frac{p_{o2}}{2} \sqrt{1 + \frac{8GBW}{p_{o2}}}. \quad (48)$$

Thus, when $p_{o2} = -8GBW$, $p_{cnd1}, p_{cnd2} \simeq p_{o2}/2 = -4GBW$. And, when $p_{o2} = -4GBW$, $p_{cnd1}, p_{cnd2} \simeq p_{o2}/2 \mp j p_{o2}/2 = -2GBW \mp j 2GBW$.

REFERENCES

- [1] Wing-Hung Ki, L. Der, and S. Lam, "Re-examination of pole splitting of a generic single stage amplifier," *IEEE Transactions on Circuits and Systems I: Fundamental Theory and Applications*, vol. 44, no. 1, pp. 70–74, 1997.
- [2] K. N. Leung and P. Mok, "Analysis of multistage amplifier-frequency compensation," *IEEE Transactions on Circuits and Systems I: Fundamental Theory and Applications*, vol. 48, no. 9, pp. 1041–1056, 2001.
- [3] A. Grasso, G. Palumbo, and S. Pennisi, "Analytical comparison of frequency compensation techniques in three-stage amplifiers," *International Journal of Circuit Theory and Applications*, vol. 36, pp. 53 – 80, 01 2008.
- [4] A. S. Sedra and K. C. Smith, *Microelectronic Circuits*, 5th ed. Oxford University Press, 2004.
- [5] P. R. Gray, *Analysis and Design of Analog Integrated Circuits*, 5th ed. Wiley Publishing, 2009.
- [6] G. F. Franklin, D. J. Powell, and A. Emami-Naeini, *Feedback Control of Dynamic Systems*, 4th ed. USA: Prentice Hall PTR, 2001.
- [7] J. Huijsing, R. Hogervorst, and K.-J. de Langen, "Low-power low-voltage vlsi operational amplifier cells," *IEEE Transactions on Circuits and Systems I: Fundamental Theory and Applications*, vol. 42, no. 11, pp. 841–852, 1995.
- [8] J. Roberge, *Operational Amplifiers: Theory and Practice*, ser. Massachusetts Institute of Technology. Radiation Laboratory. Wiley, 1975. [Online]. Available: <https://books.google.co.kr/books?id=EftSAAAAMAAJ>
- [9] K. N. Leung, P. Mok, W.-H. Ki, and J. Sin, "Three-stage large capacitive load amplifier with damping-factor-control frequency compensation," *IEEE Journal of Solid-State Circuits*, vol. 35, no. 2, pp. 221–230, 2000.
- [10] B. Ahuja, "An improved frequency compensation technique for cmos operational amplifiers," *IEEE Journal of Solid-State Circuits*, vol. 18, no. 6, pp. 629–633, 1983.

- [11] P. J. Hurst, S. H. Lewis, J. P. Keane, F. Aram, and K. C. Dyer, "Miller compensation using current buffers in fully differential cmos two-stage operational amplifiers," *IEEE Transactions on Circuits and Systems I: Regular Papers*, vol. 51, no. 2, pp. 275–285, 2004.
- [12] Feng-Tso Chien and Yi-Jen Chan, "Bandwidth enhancement of transimpedance amplifier by a capacitive-peaking design," *IEEE Journal of Solid-State Circuits*, vol. 34, no. 8, pp. 1167–1170, 1999.
- [13] M. Kim and S. Cho, "A single bjt bandgap reference with frequency compensation exploiting mirror pole," *IEEE Journal of Solid-State Circuits*, vol. 56, no. 10, pp. 2902–2912, 2021.



Myungjun Kim received the Ph.D. degree in electrical engineering from Korea Advanced Institute of Science and Technology (KAIST), Daejeon, Korea, in Feb, 2022.

His Ph.D. study has focused on the stability analysis and the development of the methodology for frequency compensation of various *linear* analog integrated circuits (ICs) such as Badngap reference and (output-capacitorless) low-dropout regulator. His research interests also include the exploration for (Hopf) bifurcation and chaos that can occur in

modern analog CMOS ICs from the *nonlinear* dynamical system theory standpoint.

He is currently working at the Memory Division, Samsung Electronics, Hwaseong, South Korea, as an analog IC designer. Dr. Kim also serves as a reviewer of IEEE TRANSACTIONS ON CIRCUITS AND SYSTEMS—I: REGULAR PAPERS and IEEE TRANSACTIONS ON CIRCUITS AND SYSTEMS—II: EXPRESS BRIEFS.